RESEARCH ARTICLE

Regulation of the swimming kinematics of lampreys *Petromyzon marinus* across changes in viscosity

Eric D. Tytell[1,*], Lauren O. Cooper[1], Yuexia Luna Lin[2] and Pedro M. Reis[2]

ABSTRACT

The bodies of most swimming fishes are very flexible and deform as result of both external fluid dynamic forces and internal musculoskeletal forces. If fluid forces change, the body motion will also change unless the fish senses the change and alters its muscle activity to compensate. Lampreys and other fishes have mechanosensory cells in their spinal cords that allow them to sense how their body is bending. We hypothesized that lampreys (*Petromyzon marinus*) actively regulate body curvature to maintain a fairly constant swimming waveform even as swimming speed and fluid dynamic forces change. To test this hypothesis, we measured the steady swimming kinematics of lampreys swimming in normal water, and water in which the viscosity was increased by 10 or 20 times by adding methylcellulose. Increasing the viscosity over this range increases the drag coefficient, potentially increasing fluid forces up to 40%. Previous computational results suggested that if lampreys did not compensate for these forces, the swimming speed would drop by about 52%, the amplitude would drop by 39%, and posterior body curvature would increase by about 31%, while tail beat frequency would remain the same. Five juvenile sea lampreys were filmed swimming through still water, and midlines were digitized using standard techniques. Although swimming speed dropped by 44% from 1× to 10× viscosity, amplitude only decreased by 4%, and curvature increased by 7%, a much smaller change than the amount we estimated if there was no compensation. To examine the waveform overall, we performed a complex orthogonal decomposition and found that the first mode of the swimming waveform (the primary swimming pattern) did not change substantially, even at 20× viscosity. Thus, it appears that lampreys are compensating, at least partially, for the changes in viscosity, which in turn suggests that sensory feedback is involved in regulating the body waveform.

KEY WORDS: Anguilliform swimming, Body waveform, Fluid dynamic forces, Proprioception

INTRODUCTION

Most swimming fishes have flexible bodies (Long, 1998; Tytell et al., 2018). Internally, they use their muscles to produce forces to bend their bodies, but external fluid dynamic forces also can cause the body to bend (e.g. Beal et al., 2006). At a mechanical level, the body waveform is thus an emergent property of the balance between internal muscular forces and external fluid forces (Tytell et al., 2010).

At the same time, fish also have proprioceptive sensory receptors that detect how the body is bending. Lampreys have well-described 'edge cells': mechanoreceptive neurons located within the spinal cord that detect stretch on the edges of the cord (Massarelli et al., 2017; Grillner et al., 1984). Recently, similar neurons called intraspinal lateral proprioceptors (ILPs) were described in the spinal cord of zebrafish (Picton et al., 2021). Both types of proprioceptors make a negative feedback loop. They respond to stretching on one side of the body (the convex side of the bend) and inhibit interneurons on the opposite side (the concave side) (Picton et al., 2021; Viana Di Prisco et al., 1990), ultimately reducing muscle activity on the concave side and thus decreasing curvature. In swimming zebrafish, when the ILP cells are disabled, the animals can swim but have higher body curvature (Picton et al., 2021).

It may be that these proprioceptors are not only involved in local feedback regulation of curvature but, in fact, also help to regulate a more global pattern of body bending across the entire body. First, these proprioceptors do not just act locally; they are connected to each other and to other interneurons over substantial distances (Picton et al., 2021; Rovainen et al., 1973). Moreover, proprioceptors in more caudal locations have different effects on the swimming rhythm from those in more rostral locations (Tytell and Cohen, 2008; Hsu et al., 2013). These rostro-caudal differences may help to maintain efficient swimming by contributing to a phase offset between muscle activity and body bending that increases caudally (Tytell and Cohen, 2008; Williams et al., 1989).

Together, these studies of the distributed (non-local) effects of proprioceptors lead to the hypothesis that fish may actively regulate not just local curvature but the entire body waveform using feedback from proprioceptive sensors. Lampreys and eels, for example, tend to maintain slightly more than one full bending wave on their bodies, regardless of swimming speed (Williams et al., 1989; Tytell, 2004). Fluid dynamic forces will tend to increase quadratically as swimming speed increases (Batchelor, 1973). Without feedback control, passively flexible panels tend to decrease wavelength as the speed increases (Hoover et al., 2018; Quinn et al., 2014). As fish tend to maintain wavelength as swimming speed changes (Wardle et al., 1995; Videler, 1993), they may have to increase muscle force as speed increases in order to maintain body wavelength.

An alternative hypothesis is that fish may regulate their swimming speed, which may lead to changes in the body waveform as the environment changes. They can sense their speed using vision (Coombs et al., 2020; Portugues and Engert, 2011) or the lateral line, a sensory system that responds to flow over the fish's body (Coombs et al., 2014). In teleost fishes, but not lampreys, the brain can modulate the sensitivity of lateral line receptors via efferent nerve connections, which are thought to increase the sensitivity of the lateral line to detect flow patterns from other animals or objects nearby. Even with this

[1]Department of Biology, Tufts University, Medford, MA 02155, USA. [2]Flexible Structures Laboratory, École polytechnique fédérale de Lausanne, 1015-Lausanne, Switzerland.

*Author for correspondence (eric.tytell@tufts.edu)

E.D.T., 0000-0002-6603-9448; Y.L.L., 0000-0003-4073-7974; P.M.R., 0000-0003-3984-828X

modulation, the lateral line also responds to the animal's own swimming motion (Mensinger et al., 2019), which may explain why it is important for rheotaxis (Suli et al., 2012; Montgomery et al., 1997) and may help to regulate swimming speed (Mekdara et al., 2021).

One way to probe these interactions is to alter the fluid dynamic forces acting on the animal by changing the viscosity. The relative importance of inertial forces compared with viscous forces is quantified by the Reynolds number:

$$Re = \frac{\rho U L}{\eta}, \qquad (1)$$

where ρ and η are the fluid's density and viscosity, respectively, and U and L are a characteristic speed and length. At high Reynolds number ($Re \gg 1$), inertial forces dominate. For the forces on the tail, the important Reynolds number is the one related to the side-to-side motion of the tail, not the forward swimming speed. Based on data from swimming eels (Tytell, 2004), this Re_{tail} is approximately 1000 at a swimming speed of $1\,L\,s^{-1}$. Even at this high Reynolds number, viscosity has an effect because the drag on the body depends on viscosity. For example, if we approximate a lamprey's body as a cylinder moving from side to side, then the drag coefficient C_D is:

$$C_D \approx 1 + \sqrt{\frac{8}{Re_{tail}}} \qquad (2)$$

(following Hoerner, 1965). At $Re_{tail} \approx 1000$, C_D should be approximately 1.09. If we increase viscosity 10 times, assuming tail beat frequency and amplitude remain the same, then Re_{tail} drops to ~100, and C_D will be approximately 1.28.

Others have used changes in viscosity to probe sensorimotor control in swimming fishes. Recently, Lutek and Standen (2021) examined swimming in *Polypterus senegalus* at viscosity ranging from normal (1 cP) to 40 cP. They found that these fish maintain speed quite effectively, possibly as a result of a substantial increase in tail beat frequency and muscle activation intensity. Horner and Jayne (2008) saw similar effects in lungfish *Protopterus annectens* in viscosities up to 1000 cP: an increase in swimming speed as viscosity increases, coupled with increases in tail beat frequency and muscle activation intensity. Both studies found a decrease in the stride length, the distance traveled per tail beat, and an increase in body curvature, particularly near the tail.

At much smaller Re, the nematode *Caenorhabditis elegans* changes its movement depending on viscosity, decreasing body wavelength as viscosity increases, from swimming with a wavelength of about $1.2\,L$ in normal water to about $0.9\,L$ at about $12\times$ viscosity (Backholm et al., 2015), and then shifting to a crawling pattern at very high viscosities (Boyle et al., 2012). Based on a computational model, Boyle et al. (2012) argued that these shifts depend on proprioceptive sensing.

Computationally, Tytell et al. (2010) examined the effects of changing viscosity in a model of a swimming lamprey with a flexible body, coupled to its fluid environment, but without any sensory feedback (Fig. 1). At $10\times$ normal viscosity, the body amplitude and wavelength decrease, resulting in much higher curvature near the tail (Fig. 1). Swimming speed drops to less than half (Fig. 1B), wavelength decreases from about $0.8\,L$ to $0.6\,L$, and curvature near the tail increases by 31%.

Living lampreys, however, have proprioceptors, including edge cells and the lateral line system. In particular, the lateral line system of lampreys lacks the efferent connections present in teleosts (Ayali et al., 2009), and thus may respond primarily to the body's own bending movements (Ayali et al., 2009). Thus, we hypothesize that
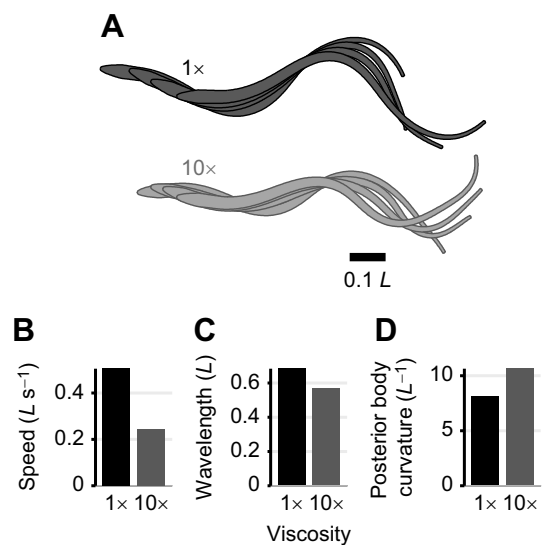
Fig. 1. Predicted changes in swimming kinematics in high-viscosity fluid based on a computational model of a swimming lamprey without sensory feedback. (A) Snapshots of movement during half a tail beat cycle at 1× and 10× viscosity. (B) Swimming speed. (C) Body wavelength. (D) Curvature in the posterior 20% of the body. Based on simulations from Tytell et al. (2010).

lampreys use their proprioceptors to maintain body waveform as external conditions change. Based on this, we predicted no substantial decrease in body wavelength and no substantial increase in body curvature as the viscosity is modified. Therefore, we examined sea lampreys, *Petromyzon marinus*, swimming in viscous fluids from 1 cP to 20 cP.

MATERIALS AND METHODS
Animals
Five juvenile lampreys *Petromyzon marinus* Linnaeus 1758 (Acme Lamprey Company, Harrison, ME, USA) were used in the experiments. The lampreys were housed in tanks with a temperature of 4°C. Before each experiment, the animal was gradually acclimated to room temperature (20°C) water over a period of at least 24 h. All procedures were approved by the Tufts University Institutional Animal Care and Use Committee (protocol M2012-145).

Fig. 2 shows the filming configuration. Each individual lamprey was placed in a 60 cm×30 cm tank, filled with water to a depth of about 10 cm. To elicit straight steady swimming, a 'funnel' was constructed that would guide the lamprey to the center of the tank. A ventral view of the swimming was captured using a high-speed camera at 50 frames s^{-1} (PCO.edge, PCO, Inc., Kelheim, Germany).

Viscosity manipulation
Each lamprey was recorded swimming in three different water viscosities: 1, 10 and 20 cP, where normal water at a temperature of 20°C has a viscosity of 1 cP. Higher viscosity solutions were produced by dissolving methylcellulose (product number M0512, Sigma-Aldrich, St Louis, MO, USA) in water at concentration of 0.4% and 0.7%. At the concentration necessary for this experiment, these methylcellulose solutions will exhibit Newtonian behavior, with constant viscosity as shear increases (Herráez-Domínguez et al., 2005). A falling-ball viscometer (Gilmont size 2 viscometer, Fisher Scientific, Pittsburgh, PA, USA) was used to confirm the viscosity of the solutions.
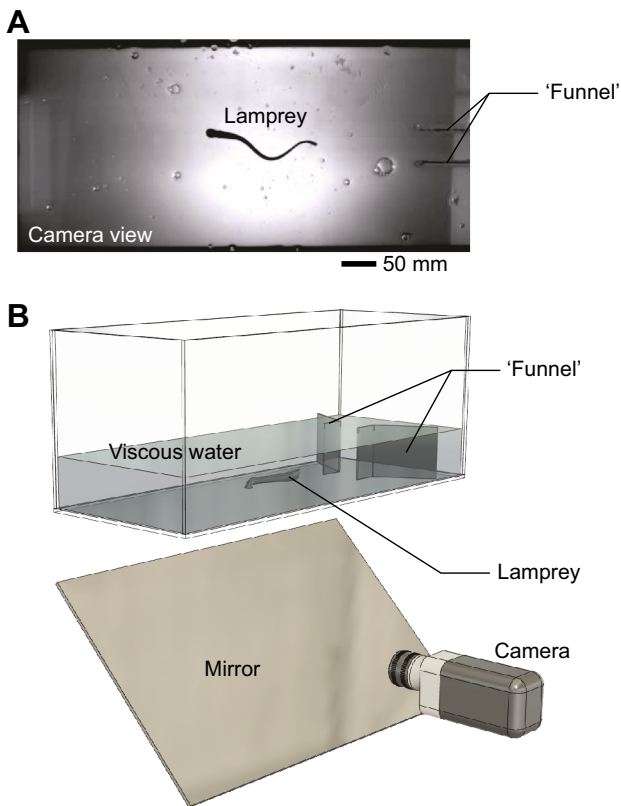
Fig. 2. Filming setup. (A) Sample frame from video. (B) Schematic diagram of filming setup, showing the tank with the 'funnel' that guides the lamprey to swim in the center of the frame. The ventral video is taken through a mirror.

Experimental protocol

Each lamprey was filmed swimming in the three viscosities for 11 trials per each viscosity, starting in normal water and then increasing viscosity. After each of the high-viscosity trials, another 4 trials in normal water were performed. Between each trial at high viscosity, the lamprey was taken out of the viscous solution and allowed to rest for at least 5 min in an oxygenated normal water solution.

Animals were first placed in the wide region of the 'funnel'. Usually they swam out volitionally, but occasionally we encouraged them to swim by gently prodding them with a wooden dowel. We were aiming for trials in which the animal did not turn substantially. Trials in which they turned left or right and reached the side walls of the tank in fewer than 2 tail beats were excluded, but they usually represented less than 10% of trials. No individuals were excluded.

Video analysis

Each video was digitized in a semi-automatic way using a custom program in Matlab (as in Tytell and Lauder, 2004). The head and tail were identified manually, and then 20 evenly spaced points were identified along the body from head to tail.

Further kinematic parameters were estimated using R (version 4.1.2; http://www.R-project.org/). First, the center of mass (COM) was estimated, assuming that the body has constant density, uniform height and varying width:

$$x_{COM} = \frac{\int_0^L \mathbf{x}(s) h w(s) \, ds}{\int_0^L h w(s) \, ds}, \quad (3)$$

where $\mathbf{x}(s)$ is the (x, y) coordinate of the midline as a function of arc length s, and h and $w(s)$ are the height and width of the body at a

position s. From the location of the COM, we then take a central difference derivative to estimate the swimming velocity U.

We used a singular value decomposition (SVD) to estimate the primary axis of the body, centered on the COM. We had $M=20$ points, equally spaced along the lamprey's body, with spatial coordinates (x_m, y_m), $m=1…M$ recorded at discrete time points t_i, $i=1…N$. At each time point, we subtracted the location of the COM, then identified the principal axis of the body by applying the SVD to the $2 \times M$ matrix of x and y coordinates:

$$\mathbf{X} = \begin{pmatrix} x_1^c(t) & … & x_M^c(t) \\ y_1^c(t) & … & y_M^c(t) \end{pmatrix}, \quad (4)$$

where $x_m^c = x_m - x_{COM}$ and $y_m^c = y_m - y_{COM}$. The SVD gives us matrices $\mathbf{A}\Sigma_{\mathbf{X}}\mathbf{B}^T$ where $\mathbf{A} \in \mathbb{R}^{2 \times 2}$. The first column of $\mathbf{A}$ is the principal axis of the body, $\mathbf{x}_p = (x_p, y_p)$. We then constructed the excursion z_m of each body point perpendicular to the main axis, $z_m(t) = -x_m^c(t)y_p(t) + y_m^c(t)x_p(t)$.

We tracked peaks in the excursion z_m to estimate body wave speed V, and the body amplitude A is the peak in the excursion at a point. Tail beat frequency f was estimated based on the time difference between successive excursion peaks at the tail. Based on these measurements, we calculated non-dimensional parameters. Stride length U^* is the distance relative to body length traveled per tail beat: $U^* = U/(Lf)$. Strouhal number St is a measure of efficiency: $St = 2fA/U$, where peak efficiency is typically around $St = 0.3$ (Triantafyllou et al., 1993).

Complex orthogonal decomposition

To examine the body waveform as a function of viscosity, we performed a complex orthogonal decomposition (COD) (Feeny, 2008; Feeny and Feeny, 2013; Leroy-Calatayud et al., 2022), which extracts not only standing wave but also traveling wave characteristics in temporal data at distributed positions.

To perform the COD, we first organized the excursion of each point relative to the main body axis and the COM into a data matrix with real values:

$$\mathbf{Z} = \begin{pmatrix} z_1(t_1) & z_1(t_2) & … & z_1(t_N) \\ \vdots & & & \vdots \\ z_M(t_1) & z_M(t_2) & … & z_M(t_N) \end{pmatrix}, \quad (5)$$

where $\mathbf{Z}$ has dimension $M \times N$. Each row of $\mathbf{Z}$ corresponds to data from a single point over time, which we denote as $\bar{z}_m$, where the bar on top indicates a vector in time.

We transformed this real-valued matrix into a complex one using the Hilbert transform $\mathcal{H}(\cdot)$. The Hilbert transform is commonly used to produce a complex-valued waveform, shifted 90 deg in phase relative to the original signal. For example, the Hilbert transform of $\cos(2\pi x/\lambda)$ would be $\sin(2\pi x/\lambda)$, where λ is the wavelength. We constructed $\bar{z}_m^* = \bar{z}_m + i\mathcal{H}(\bar{z}_m)$ and stacked them to produce the complex data matrix $\mathbf{Z}^* = (\bar{z}_1^* … \bar{z}_M^*)^T$. The complex correlation matrix is defined as:

$$\mathbf{R} = \mathbf{Z}^* \overline{\mathbf{Z}}^{*T} \in \mathbb{C}^{M \times M}. \quad (6)$$

The SVD on $\mathbf{R}$, $\mathbf{R} = \mathbf{V}\Sigma_R\overline{\mathbf{V}}^T$, yields singular vectors $\mathbf{V} \in \mathbb{R}^{M \times M}$ and singular values of $\mathbf{R}$ as the diagonal of Σ_R. We then defined $\mathbf{Q} = \overline{\mathbf{V}}^T\mathbf{Z}^*$, $\mathbf{Q} \in \mathbb{C}^{M \times N}$, the complex modal coordinates.

These quantities have physical meanings: (1) columns of $\mathbf{V}$ are the complex orthogonal modes, which are the basis functions that describe the body waveform, (2) the non-negative, real singular values in Σ_R indicate importance of the modes, (3) the rows of $\mathbf{Q}$ contain the

time-dependent complex amplitudes of the corresponding mode. Thus, the first complex orthogonal mode is the most dominant, and it largely captures the waveform of a bending body (Feeny and Feeny, 2013).

The mode can be considered as a discrete curve $\bar{\gamma}$ consisting of points γ_m, $m \in 1 \ldots M$ in the complex plane, each corresponding to a point with arc length s_m along the animal body from head to tail. The wavelength λ of the first mode can be estimated by computing the winding number n of the curve $\bar{\gamma}$ (Feeny and Feeny, 2013), which is the number of times a planar curve circles around a point. Consider the point $w = \frac{1}{M} \sum_{m=1}^{M} \gamma_m$, we define winding number around w as $n(\bar{\gamma}, w) \equiv n(s_m, w) = (\theta(\gamma_M) - \theta(\gamma_1))/2\pi$, where θ is the polar angle in the polar coordinate system centered at w (Garling, 2014). Following the previous example, if $\bar{\gamma}$ is the discrete complex harmonic signal $\gamma_m = \cos(kx_m) - i\sin(kx_m)$, $m = 1 \ldots M$, and contains exactly one wavelength, i.e. $\gamma_1 = \gamma_M$, then $n(\bar{\gamma}, w) = 1$. Furthermore, if $\bar{\gamma}$ is a discretized harmonic signal sampled at uniformly spaced points, then winding number and wavelength can be related by $\lambda = L/n$. Thus, winding number $n > 1$ indicates that the body length is longer than the wavelength, $L > \lambda$, and vice versa. However, because the lamprey body waveform is not sinusoidal, we propose an alternative way of relating wavelength to winding number. After computing the winding number at each point of $\bar{\gamma}$, the critical body arc length $s_c \in [0, L]$ at which $n = 1$ is found by linear interpolation, providing an estimate of the wavelength $\lambda \approx s_c$. Although not observed in our dataset, in the case of $n < 1$, $n(s_m, w)$ can be linearly extrapolated to find the length s_c at which $n = 1$.

The traveling index of a mode j, $j = 1 \ldots M$ indicates the degree to which a waveform can be described by a traveling versus a standing wave. For the jth column of $\mathbf{V}$, $\bar{v}_j$, a two-column matrix with its real (Real) and imaginary (Imag) parts is constructed, i.e. $\mathbf{T}_j = [\text{Real}(\bar{v}_j)^{\text{T}} \text{Imag}(\bar{v}_j)^{\text{T}}]$. The traveling index of this mode is defined as $\mathcal{I} = \text{Cond}(\mathbf{T}_j)^{-1}$, i.e. the inverse of the condition number of $\mathbf{T}_j$. A traveling index $\mathcal{I} = 1$ indicates a perfect traveling wave and $\mathcal{I} = 0$ is a perfect standing wave.

Statistics
To identify differences in swimming kinematics at different viscosities, we fitted kinematic data to a mixed model containing viscosity as a fixed, categorical effect and random intercept for each individual (in R notation: value ~ viscosity + (1 | indiv)), where 'value' is a kinematic variable such as swimming speed. Each value in the model is a mean across a trial. We used R (version 4.1.2; http://www.R-project.org/) with the lme4 package (version 1.1.27.1; Bates et al., 2015) and lmerTest (version 3.1.3; Kuznetsova et al., 2017) to estimate *P*-values, and emmeans (version 1.7.0; https://CRAN.R-project.org/package=emmeans) to estimate marginal means and effect sizes. We performed pairwise multiple comparisons with a Tukey correction using emmeans.

In the text, we report values as means±s.d. In the figures, we show marginal means from the statistical models ±s.e.m., with brackets indicating significant differences relative to control (1 cP).

RESULTS
We recorded 222 swimming bouts from five individual lampreys (mean total length 150±4 mm), consisting of 1507 total tail beats. We had 96 trials in normal water, 54 in 10 cP and 72 in 20 cP. Each trial consisted of 4 tail beats on average in normal water, 7 in 10 cP and 10 in 20 cP.

Swimming is slower and less efficient at high viscosity
We first extracted swimming kinematics using video analysis. Fig. 3 shows example midlines at each of the three viscosities. One can see
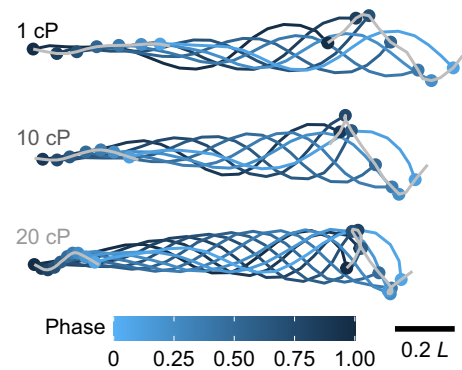
Fig. 3. Swimming kinematics and undulation amplitude as viscosity changes. Representative midlines at 7 phases throughout a full tail beat cycle in the three different water viscosities: 1, 10 and 20 cP. Circles show the head and tail location and are connected by light gray lines.

that the swimming speed and, thus, the stride length decreased substantially as viscosity increased. Frequency and body wave speed varied proportionally to swimming speed (Fig. 4A,B), but the relationship was different at different viscosities. In particular, at a higher viscosity, the same frequency or body wave speed produced a much lower swimming speed. Stride length, or the fraction of a body length traveled in each tail beat, increased with swimming speed, but was generally much lower at higher viscosity (Fig. 4C). Body wavelength (Fig. 4D) did not vary substantially with speed.

Although swimming speed depends on several kinematic parameters, such as tail beat frequency, the largest effect on kinematics is the viscosity. Swimming speed itself arises as the result of interactions between the kinematics and the environment. We next investigated in detail the changes in the kinematics as a function of viscosity. Fig. 5 shows the average kinematic patterns for each individual as viscosity changes. Speed decreased significantly from 1.5±0.4 L s^{-1} (mean±s.d.) to 0.3±0.2 L s^{-1} at the highest viscosity, an effect size of −3.79 (Fig. 5A), corresponding to a decrease from Re=30,000±10,000 to 400±200 (Fig. 5B). Frequency changed much less: from 3.1±0.9 Hz in normal water to 2.2±0.8 Hz at the highest viscosity, a statistically significant change with an effect size of −0.99 (Fig. 5C). See Table 1 for a statistical summary.

These changes seem to correspond to a decrease in the effectiveness of swimming at higher viscosity (Fig. 6). The stride length decreases significantly from 0.51±0.07 L to 0.14±0.03 L. Strouhal number St increased significantly, from 0.33±0.05 under control conditions to 0.91±0.15 at the highest viscosity.

Body waveform does not change substantially
Although these kinematic parameters changed, the overall body waveform was quite similar across viscosities and did not show the large changes predicted by the computational model (Fig. 1). Fig. 7A shows the changes in the amplitude envelope as a function of position along the body. Amplitudes were slightly smaller along most of the body at the highest viscosity. The average amplitude across the entire body (Fig. 7B) did not change significantly up to 10 cP and only decreased by 21% at the highest viscosity. These values correspond to tail tip amplitudes of 0.082±0.014 L under control conditions and 0.06±0.011L at 20 cP. In contrast, the simulation's body amplitude dropped by 39% from 0.090 L in normal water to 0.055 L with a change of only 10 cP.

To further quantify the changes in body waveform across viscosities, we performed COD analysis for each swimming trial,
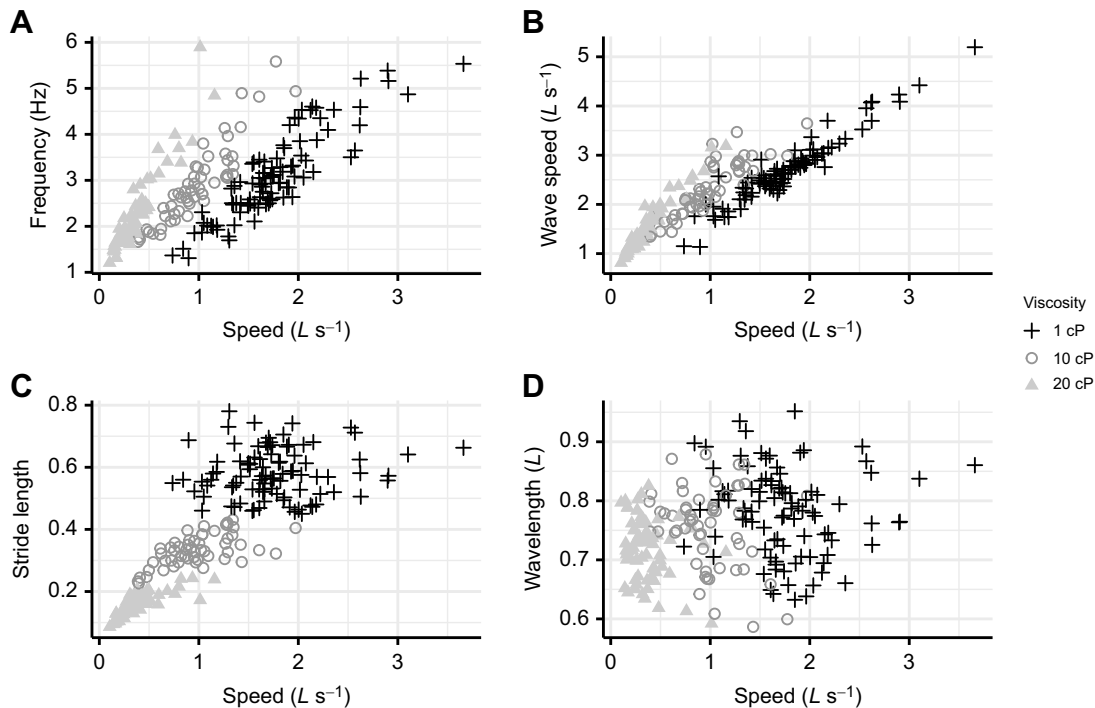
Fig. 4. Viscosity affects the relationship between swimming kinematics and speed. (A) Frequency, (B) body wave speed, (C) stride length and (D) body wavelength, all relative to swimming speed. Each point represents the mean across one swimming trial.

which produces separate patterns of body bending. Fig. 8A shows the first mode for each individual in each viscosity, which is the dominant mode that captures the undulating swimming gait.

The wavelength calculated from the first mode shortened only slightly at higher viscosity (Fig. 8A,C), decreasing by 5% on average at 10 cP (0.76 ± 0.04 L to 0.72 ± 0.06 L), an effect size of -0.7. Even at 20 cP, the wavelength was only 10% lower than that under control conditions. This decrease depended substantially on individual variability, with only two individuals dropping more than 0.05 L from control to the 10 cP (green and red points in Fig. 8C). Again, the simulation's kinematics changed much more substantially over a smaller viscosity range, with the wavelength decreasing by 28% (0.83 L to 0.60 L) from control to 10 cP. Curvature in the posterior body (Fig. 8D) increased by 7% on average at 10 cP, much less than the change in the simulation, which increased by 31%.

The traveling index $\mathcal{I}$, which quantifies how well the mode is described as a traveling versus standing wave, also changed little

across viscosities (Fig. 8B). Traveling index $\mathcal{I}=1$ indicates a perfect traveling wave. Our measured traveling index values of the first mode stayed close to 1, regardless of viscosity, and in fact increased slightly from 0.790.05 under control conditions to 0.82 ± 0.06 at the highest viscosity.

DISCUSSION

We examined juvenile lampreys *Petromyzon marinus* swimming in water, in which viscosity was artificially increased, as a way to probe the sensorimotor control of body waveform. Specifically, we asked to what extent do lampreys use sensory feedback to maintain a constant waveform as swimming conditions vary? We found that swimming is less effective as viscosity increases: it is slower, with a lower stride length, and a higher Strouhal number. Even so, the waveform does not change very much. The average body amplitude decreased slightly at high viscosity, and the body wavelength shortened, but not nearly as much as they did in a computational swimmer that had no feedback (from Tytell et al., 2010). We see this
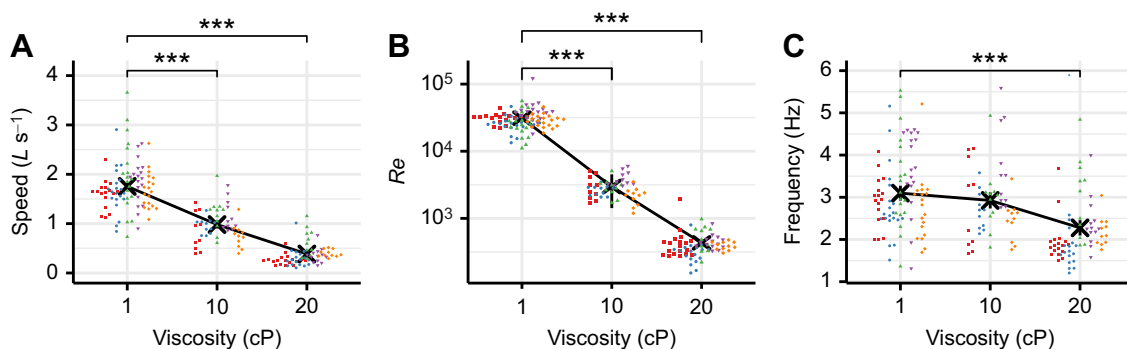
Fig. 5. Swimming speed, Reynolds number and tail beat frequency decrease as viscosity increases. (A) Swimming speed. (B) Reynolds number (Re). (C) Tail beat frequency. In each plot, individuals are shown with different colors, and each point represents the mean across one swimming trial. ***$P<0.001$.

**Table 1. Statistical tests on kinematic data of lampreys swimming at various viscosities**

	$F^{§}$	df_1	df_2	P	Effect size[‡] 10–1 cP	Effect size[‡] 20–1 cP
Swimming speed	281	2	211.4	<0.001	**−2.10*****	**−3.72*****
Tail beat amplitude	11.5	2	211.1	<0.001	0.37	−0.49*
Tail beat frequency	20.6	2	211.3	<0.001	−0.21	**−0.99****
Body wave speed	81.6	2	211.3	<0.001	*−0.66**	**−2.01*****
Stride length	1120	2	211.3	<0.001	**−4.34*****	**−7.41*****
Strouhal number	814	2	207.2	<0.001	**2.41*****	**6.43*****
Traveling wave index	9.12	2	202.3	<0.001	0.33	*0.69***
Posterior body curvature	22.2	2	211.1	<0.001	0.48*	**1.06****

[‡]Effect size for differences in viscosity. [§]Statistical F parameter with degrees of freedom df_1 and df_2. Large effects are in bold; medium are in italic. Pairwise comparisons: *$P<0.05$, **$P<0.01$, ***$P<0.001$.

as evidence that lampreys do regulate body waveform but are unable to fully compensate for the change in forces at very high viscosity.

Regulation of swimming speed

Lampreys do not appear to regulate their swimming speed as viscosity increases. Speed drops by 79% at the highest viscosity, and frequency by 27%, corresponding to substantial drops in stride length and increases in Strouhal number (Fig. 6). They can likely
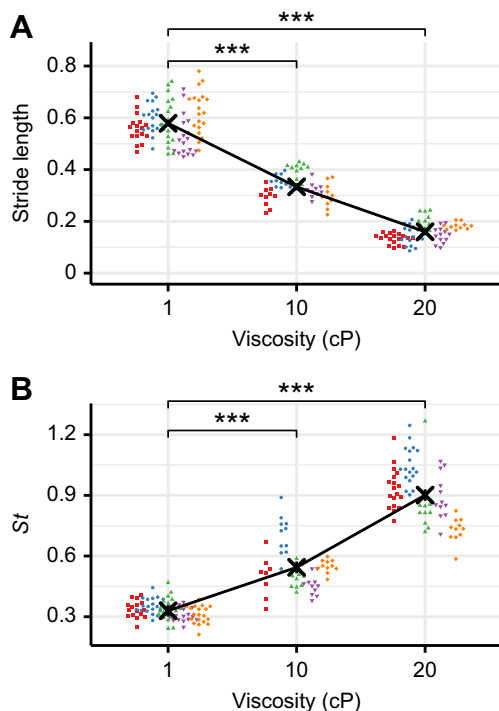
Fig. 6. Swimming becomes less effective as viscosity increases. (A) Stride length, the measure of body lengths traveled per tail beat. (B) Strouhal number (St). In each plot, individuals are shown with different colors, and each point represents the mean across one swimming trial. ***$P<0.001$.

sense their swimming speed, either visually (Coombs et al., 2020) or through the lateral line sense (Ayali et al., 2009). Our study animals were juvenile lampreys, which are fully metamorphosed adults that are not yet reproductively mature (Manzon et al., 2015), with a fully developed nervous systems, eyes and lateral line system (Cohen et al., 1990; Manzon et al., 2015). Unlike larval lampreys (also called 'ammocoetes'), juveniles swim in a well-coordinated way (McClellan et al., 2016). Although mean frequency does drop at the highest viscosity, the range of frequencies used does not change much; instead, the same frequency produces a much slower swimming speed at high viscosity, resulting in nearly non-overlapping stride lengths at the different viscosities (Fig. 4).

Other fishes, when challenged with higher viscosity, do seem to regulate swimming speed. In particular, lungfish *Protopterus annectens* do not swim slower when placed in fluid up to 1000 cP; they may even swim faster, though the trend was not significant (Horner and Jayne, 2008). They achieve this by nearly doubling tail beat frequency (Horner and Jayne, 2008). However, lungfish may be adapted to movement through high-viscosity fluids. Under normal conditions, they live in ponds that dry up and become muddy, and they may have to move through the mud, which can reach very high viscosity (100–1000 cP or more; Horner and Jayne, 2008). They may thus have developed a strategy for compensating for high viscosity (Horner and Jayne, 2008). Bichirs *Polypterus senegalus* have a similar response, increasing tail beat frequency and maintaining swimming speed at viscosities up to 40 cP (Lutek and Standen, 2021). For both lungfish and bichirs, maintaining swimming speed requires a substantial increase in muscle activity (Horner and Jayne, 2008; Lutek and Standen, 2021)

Sensory regulation of body kinematics

When fish swim, they produce forces internally with their muscles and as a result of the elastic properties of their bodies. At the same time, the fluid around them produces forces back on the body. The resulting swimming motion and body deformation is, therefore, an emergent property of this coupled interaction of passive body mechanics, active muscle forces and fluid reaction forces (Tytell et al., 2010).

Fish sense body deformation and can respond to it via proprioceptive sensory cells. There are several known classes of such cells that can respond to deformation, including edge cells in lampreys (Grillner et al., 1984; Viana Di Prisco et al., 1990) and ILP cells in zebrafish (Picton et al., 2021). Both types of cell have the effect of reducing extreme curvature. Indeed, when the ILPs are disabled genetically, zebrafish swim with much higher body curvature and poorer coordination of their trajectory (Picton et al., 2021). The nematode *C. elegans* likely also possesses proprioceptive mechanosensory cells (Denham et al., 2018), which seem to be important for gait modulation as viscosity changes (Boyle et al., 2012).

Edge cells and ILPs send processes that extend rostrally for many segments along the spinal cord (Rovainen, 1974; Picton et al., 2021). Previous studies (Viana Di Prisco et al., 1990; Picton et al., 2021) have examined their effects on the central pattern generator circuits locally, but these long processes suggest that such cells could also have an effect on the body more widely. Indeed, the relatively small changes in swimming waveform that we observed suggest that edge cells not only influence local curvature but also may have an effect on the body waveform overall.

It is not possible to disable edge cells *in vivo*, so it is not known what a lamprey swimming without edge cells would do. However, Tytell et al. (2010) simulated a flexible swimmer, modeled on a lamprey, with no sensory feedback, and examined the effect of
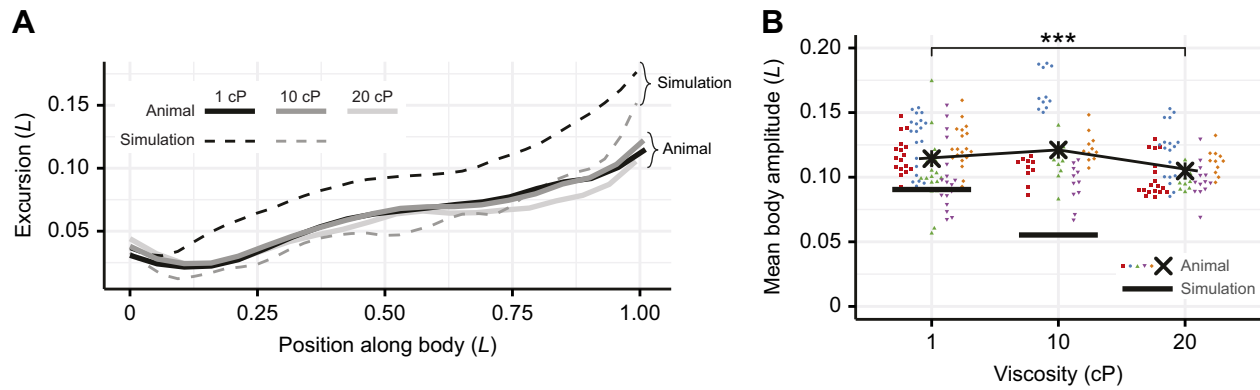
Fig. 7. Body amplitude drops slightly as viscosity increases. (A) Mean amplitude envelopes for each viscosity. For comparison, amplitudes from the simulation are shown as dashed lines. (B) Mean body amplitude. Individuals are shown with different colors, and each point represents the mean across one swimming trial. Bars represent the means from simulations. ***$P<0.001$.

changing viscosity. Without changing muscle activity, body amplitude and wavelength dropped substantially, and the curvature near the tail increased (Fig. 1). These simulation results serve as something like a null hypothesis for the current study. If lampreys did not regulate swimming waveform, we would expect to see changes similar to those found in simulation (Tytell et al., 2010). Although all of the changes we observed in real lampreys were in the same direction as those in the simulation – in particular, body amplitude and wavelength decreased and posterior curvature increased for both animals and simulations – the changes in real lampreys were much smaller than those in the simulation.

To provide more detail on lamprey swimming modes across various viscosities, we performed a complex orthogonal decomposition and calculated the traveling index of the complex swimming modes (Feeny, 2008; Feeny and Feeny, 2013), which allowed us to compare the swimming with the movement of passively flexible foils. In particular, Leroy-Calatayud et al. (2022) studied such a foil and found that the traveling index was strongly correlated with its propulsive performance: the traveling index increased as frequency increased, up to a maximum at a frequency just higher than the mechanical resonant frequency of the foil, which also
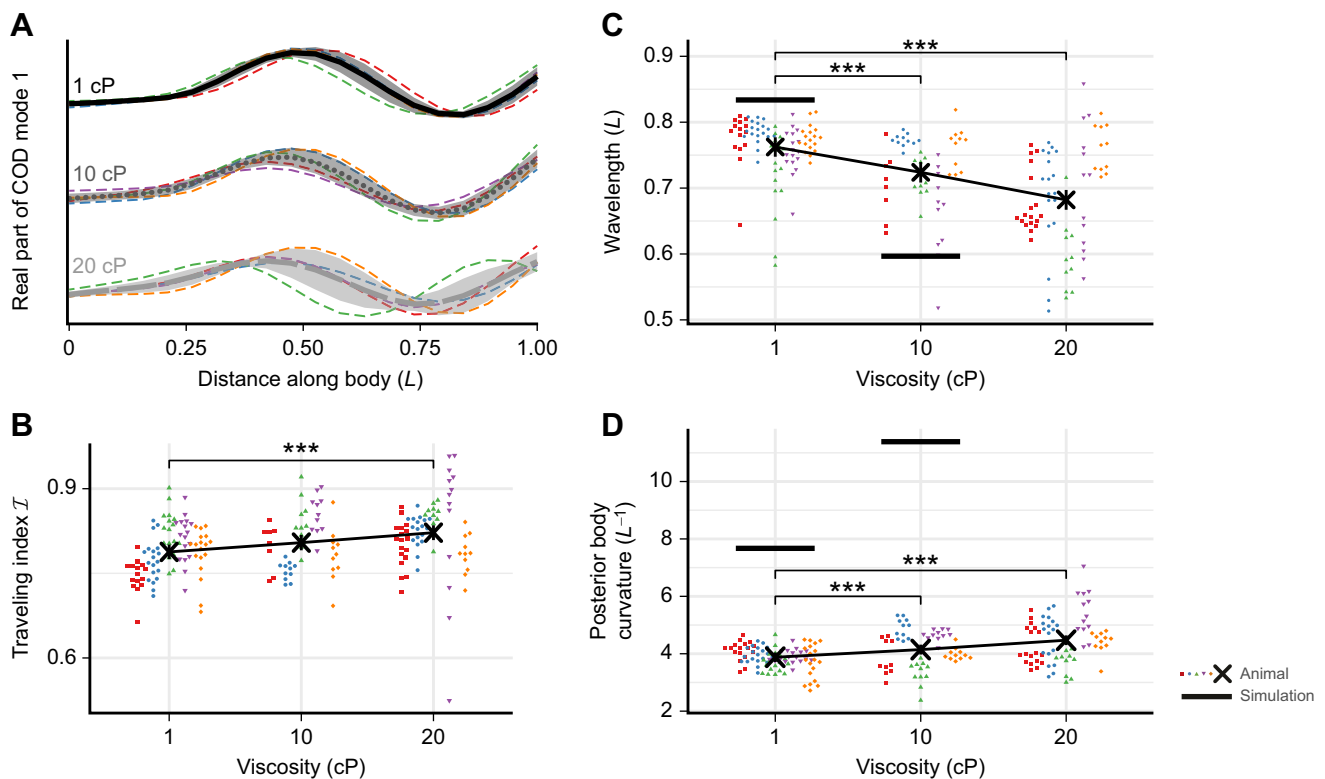
Fig. 8. Body waveform changes as viscosity increases, but not as much as for the simulated swimmer. (A) Real part of the first mode of the complex orthogonal decomposition (COD). Means for each individual are shown in color, and overall means are shown in shades of gray with a lighter region representing the standard deviation. (B) Traveling index $\mathcal{I}$. (C) Body wavelength. (D) Mean curvature in the posterior body (0.75 L to 0.95 L). In each plot, individuals are shown with different colors, and each point represents the mean across one swimming trial. Data from the simulated swimmer are show with bars. ***$P<0.001$.

corresponded to a peak in efficiency (Alben et al., 2012; Quinn et al., 2014; Paraz et al., 2016). In contrast to these passive foils, even though lampreys swimming in high viscosity fluid seem to be less efficient, the traveling index does not decrease. In fact, it increased slightly at higher viscosity (Fig. 8B). Regardless of the increased viscosity, the lamprey body waveform, a mixture of traveling and standing waves, remained stable, suggesting that lampreys are actively controlling the waveform.

We take this stability in the body waveform as evidence of partial regulation of swimming gait in lampreys. Forces on the tail are likely substantially higher at high viscosity. The Reynolds number for the body's side-to-side motion drops from 4000±1000 to 100±30. For a cylinder moving laterally, the drag coefficient in Eqn 2 would increase from 1.04 to 1.28 (Hoerner, 1965), but the speed of the tail perpendicular to its surface stays approximately the same, suggesting an increase in forces by about 23%. For the waveform changes to be as small as they were, even at 20 cP, lampreys must be activating their muscles more strongly to compensate for the increased forces. They are therefore regulating their swimming kinematics to maintain the waveform, even as fluid dynamic forces change.

Based on further comparisons with experiments and simulations of passively flexible panels, it seems likely that fishes are using sensory feedback to regulate their swimming kinematics more broadly. For example, when a passive flexible foil is heaved back and forth, its deformation waveform, and thus its swimming speed and efficiency, have been shown to vary greatly as a function of the heaving frequency (Ramananarivo et al., 2011; Alben et al., 2012; Quinn et al., 2014; Paraz et al., 2016; Piñeirua et al., 2017; Leroy-Calatayud et al., 2022; Hoover et al., 2018). As frequency increases, the swimming speed of a passive foil increases and decreases, with multiple fluid-structural resonant peaks (Hoover et al., 2018). These resonant frequencies are determined by a parameter called the 'effective flexibility' $\Pi \propto f/\sqrt{EI}$, where f is the frequency, E is the stiffness (Young's modulus) and I is related to the shape of the cross-section (the second-moment of area) (Quinn et al., 2014). One way that a fish could maintain its swimming waveform and increase speed smoothly with frequency would be to increase its effective stiffness E proportionally. Lampreys and other fishes are capable of increasing stiffness in this way by changing muscle activity (Long, 1998; Tytell et al., 2018), changes that could be driven by increases in proprioceptive feedback gain (e.g. Hamlet et al., 2018).

More broadly speaking, it is as yet unclear how to generalize and relate results obtained with passive foils with external actuation to freely swimming animals. Our work is part of a trend to use interdisciplinary techniques to understand locomotion, propulsion and biomechanics, which can lead to better designs of propulsive devices. The results we show here highlight the similarity and, more importantly, the distinctions between experimental, computational and biological systems, and indicate that feedback control of swimming waveforms may be a key difference between these systems.

Competing interests
The authors declare no competing or financial interests.

Author contributions
Conceptualization: E.D.T.; Methodology: E.D.T.; Software: E.D.T., Y.L.L.; Formal analysis: E.D.T., L.O.C., Y.L.L.; Investigation: L.O.C.; Resources: E.D.T.; Data curation: L.O.C.; Writing - original draft: L.O.C.; Writing - review & editing: E.D.T., Y.L.L., P.M.R.; Visualization: E.D.T.; Supervision: E.D.T., P.M.R.; Project administration: E.D.T.; Funding acquisition: E.D.T.

Data availability
All data and analysis scripts are available from the LabArchives database: doi:10.25833/h154-hf67.

References
Alben, S., Witt, C., Baker, T. V., Anderson, E. and Lauder, G. V. (2012). Dynamics of freely swimming flexible foils. *Phys. Fluids* **24**, 051901. doi:10.1063/1.4709477

Ayali, A., Gelman, S., Tytell, E. D. and Cohen, A. H. (2009). Lateral-line activity during undulatory body motions suggests a feedback link in closed-loop control of sea lamprey swimming. *Can. J. Zool.* **87**, 671-683. doi:10.1139/Z09-050

Backholm, M., Kasper, A. K. S., Schulman, R. D., Ryu, W. S. and Dalnoki-Veress, K. (2015). The effects of viscosity on the undulatory swimming dynamics of *C. elegans*. *Phys. Fluids 1994–Present* **27**, 91901. doi:10.1063/1.4931795

Batchelor, G. K. (1973). *An Introduction to Fluid Dynamics*. Cambridge: Cambridge University Press.

Bates, D., Mächler, M., Bolker, B. and Walker, S. (2015). Fitting linear mixed-effects models using lme4. *J. Stat. Softw* **67**, 1-48. doi:10.18637/jss.v067.i01

Beal, D. N., Hover, F. S., Triantafyllou, M. S., Liao, J. C. and Lauder, G. V. (2006). Passive propulsion in vortex wakes. *J. Fluid Mech* **549**, 385-402. doi:10.1017/S0022112005007925

Boyle, J. H., Berri, S. and Cohen, N. (2012). Gait modulation in *C. elegans*: An integrated neuromechanical model. *Front. Comput. Neurosci* **6**, 1-15. doi:10.3389/fncom.2012.00010

Cohen, A. H., Dobrov, T. A., Guan, L., Kiemel, T. and Baker, M. T. (1990). The development of the lamprey pattern generator for locomotion. *J. Neurobiol* **21**, 958-969. doi:10.1002/neu.480210703

Coombs, S., Bleckmann, H., Fay, R. R. and Popper, A. N. (ed.). (2014). *The Lateral Line System: of Springer Handbook of Auditory Research*, Vol. 48. New York, NY: Springer New York. ISBN 978-1-4614-8850-7.

Coombs, S., Bak-Coleman, J. and Montgomery, J. (2020). Rheotaxis revisited: A multi-behavioral and multisensory perspective on how fish orient to flow. *J. Exp. Biol.* **223**, jeb223008. doi:10.1242/jeb.223008

Denham, J. E., Ranner, T. and Cohen, N. (2018). Signatures of proprioceptive control in *Caenorhabditis elegans* locomotion. *Philos. Trans. R. Soc. B Biol. Sci.* **373**, 26-28. doi:10.1098/rstb.2018.0208

Feeny, B. F. (2008). A complex orthogonal decomposition for wave motion analysis. *J. Sound Vib.* **310**, 77-90. doi:10.1016/j.jsv.2007.07.047

Feeny, B. and Feeny, A. K. (2013). Complex modal analysis of the swimming motion of a whiting. *J. Vib. Acoust.* **135**, 21004. doi:10.1115/1.4023056

Garling, D. J. H. (2014). *A Course in Mathematical Analysis: Complex Analysis, Measure and Integration*, Vol. 3. Cambridge University Press. ISBN 978–1-107-65612-3.

Grillner, S., Williams, T. L. and Lagerbäck, P.-Å. (1984). The edge cell, a possible intraspinal mechanoreceptor. *Science* **223**, 500-503. doi:10.1126/science.6691161

Hamlet, C. L., Hoffman, K. A., Tytell, E. D. and Fauci, L. J. (2018). The role of curvature feedback in the energetics and dynamics of lamprey swimming: A closed-loop model. *PLOS Comput. Biol.* **14**, e1006324. doi:10.1371/journal.pcbi.1006324

Herráez-Domínguez, J. V., de León, F. G. G., Díez-Sales, O. and Herráez-Domínguez, M. (2005). Rheological characterization of two viscosity grades of methylcellulose: An approach to the modeling of the thixotropic behaviour. *Colloid Polym. Sci.* **284**, 86-91. doi:10.1007/s00396-005-1332-3

Hoerner, S. F. (1965). *Fluid-Dynamic Drag. Practical Information on Aerodynamic Drag and Hydrodynamic Resistance*. Bakersfield, CA: Hoerner Fluid Dynamics.

Hoover, A. P., Cortez, R., Tytell, E. D. and Fauci, L. J. (2018). Swimming performance, resonance, and shape evolution in heaving flexible panels. *J. Fluid Mech.* **847**, 386-416. doi:10.1017/jfm.2018.305

Horner, A. M. and Jayne, B. C. (2008). The effects of viscosity on the axial motor pattern and kinematics of the African lungfish (*Protopterus annectens*) during lateral undulatory swimming. *J. Exp. Biol.* **211**, 1612-1622. doi:10.1242/jeb.013029

Hsu, L.-J., Zelenin, P. V., Grillner, S., Orlovsky, G. N. and Deliagina, T. G. (2013). Intraspinal stretch receptor neurons mediate different motor responses along the body in lamprey. *J. Comp. Neurol* **521**, 3847-3862. doi:10.1002/cne.23382

Kuznetsova, A., Brockhoff, P. B. and Christensen, R. H. B. (2017). lmerTest package: tests in linear mixed effects models. *J. Stat. Softw* **82**, 1-26. doi:10.18637/jss.v082.i13

Leroy-Calatayud, P., Pezzulla, M., Keiser, A., Mulleners, K. and Reis, P. M. (2022). Tapered foils favor traveling-wave kinematics to enhance the performance of flapping propulsion. *Phys. Rev. Fluids* **7**, 074403. doi:10.1103/PhysRevFluids.7.074403

Long, J. H. (1998). Muscles, elastic energy, and the dynamics of body stiffness in swimming eels. *Am. Zool* **38**, 771-792. doi:10.1093/icb/38.4.771

Lutek, K. and Standen, E. M. (2021). Increasing viscosity helps explain locomotor control in swimming polypterus senegalus. *Integr. Org. Biol.* **3**, obab024. doi:10.1093/iob/obab024

Manzon, R. G., Youson, J. H. and Holmes, J. A. (2015). Lamprey metamorphosis. In *Lampreys: Biology, Conservation and Control: Fish & Fisheries Series*, Vol. 1 (ed. M. F. Docker), pp. 139-214. Dordrecht: Springer. ISBN 978-94-017-9306-3.

Massarelli, N., Yau, A. L., Hoffman, K. A., Kiemel, T. and Tytell, E. D. (2017). Characterization of the encoding properties of intraspinal mechanosensory neurons in the lamprey. *J. Comp. Physiol. A* **203**, 831-841. doi:10.1007/s00359-017-1196-2

McClellan, A. D., Pale, T., Messina, J. A., Buso, S. and Shebib, A. (2016). Similarities and differences for swimming in larval and adult lampreys. *Physiol. Biochem. Zool* **89**, 294-312. doi:10.1086/686893

Mekdara, P. J., Nasimi, F., Schwalbe, M. A. B. and Tytell, E. D. (2021). Tail beat synchronization during schooling requires a functional lateral line system in giant danios, *Devario aequipinnatus*. *Integrative and Comparative Biology* **61**, 427-441. doi:10.1093/icb/icab071

Mensinger, A. F., Van Wert, J. C. and Rogers, L. S. (2019). Lateral line sensitivity in free-swimming toadfish Opsanus tau. *J. Exp. Biol.* **222**, jeb190587. doi:10.1242/jeb.190587

Montgomery, J. C., Baker, C. F. and Carton, A. G. (1997). The lateral line can mediate rheotaxis in fish. *Nature* **389**, 960-963. doi:10.1038/40135

Paraz, F., Schouveiler, L. and Eloy, C. (2016). Thrust generation by a heaving flexible foil: Resonance, nonlinearities, and optimality. *Phys. Fluids 1994–Present* **28**, 11903. doi:10.1063/1.4939499

Picton, L. D., Bertuzzi, M., Pallucchi, I., Fontanel, P., Dahlberg, E., Björnfors, E. R., Iacoviello, F., Shearing, P. R. and El Manira, A. (2021). A spinal organ of proprioception for integrated motor action feedback. *Neuron* **109**, 1188-1201.e7. doi:10.1016/j.neuron.2021.01.018

Piñeirua, M., Thiria, B. and Godoy-Diana, R. (2017). Modelling of an actuated elastic swimmer. *J. Fluid Mech* **829**, 731-750. doi:10.1017/jfm.2017.570

Portugues, R. and Engert, F. (2011). Adaptive locomotor behavior in larval zebrafish. *Front. Syst. Neurosci* **5**, 72. doi:10.3389/fnsys.2011.00072

Quinn, D. B., Lauder, G. V. and Smits, A. J. (2014). Scaling the propulsive performance of heaving flexible panels. *J. Fluid Mech* **738**, 250-267. doi:10.1017/jfm.2013.597

Ramananarivo, S., Godoy-Diana, R. and Thiria, B. (2011). Rather than resonance, flapping wing flyers may play on aerodynamics to improve performance. *Proc. Natl. Acad. Sci. USA* **108**, 5964-5969. doi:10.1073/pnas.1017910108

Rovainen, C. M. (1974). Synaptic interactions of identified nerve cells in the spinal cord of the sea lamprey. *J. Comp. Neurol.* **154**, 189-206. doi:10.1002/cne.901540206

Rovainen, C. M., Johnson, P. A., Roach, E. A. and Mankovsky, J. A. (1973). Projections of individual axons in lamprey spinal cord determined by tracings through serial sections. *J. Comp. Neurol* **149**, 193-201. doi:10.1002/cne.901490205

Suli, A., Watson, G. M., Rubel, E. W. and Raible, D. W. (2012). Rheotaxis in larval zebrafish is mediated by lateral line mechanosensory hair cells. *PLoS ONE* **7**, e29727. doi:10.1371/journal.pone.0029727

Triantafyllou, G. S., Triantafyllou, M. S. and Grosenbaugh, M. A. (1993). Optimal thrust development in oscillating foils with application to fish propulsion. *J. Fluids Struct.* **7**, 205-224. doi:10.1006/jfls.1993.1012

Tytell, E. D. (2004). The hydrodynamics of eel swimming. II. Effect of swimming speed. *J. Exp. Biol* **207**, 3265-3279. doi:10.1242/jeb.01139

Tytell, E. D. and Cohen, A. H. (2008). Rostral versus caudal differences in mechanical entrainment of the lamprey central pattern generator for locomotion. *J. Neurophysiol.* **99**, 2408-2419. doi:10.1152/jn.01085.2007

Tytell, E. D. and Lauder, G. V. (2004). The hydrodynamics of eel swimming. I. Wake structure. *J. Exp. Biol.* **207**, 1825-1841. doi:10.1242/jeb.00968

Tytell, E. D., Hsu, C.-Y., Williams, T. L., Cohen, A. H. and Fauci, L. J. (2010). Interactions between internal forces, body stiffness, and fluid environment in a neuromechanical model of lamprey swimming. *Proc. Natl. Acad. Sci. USA* **107**, 19832-19837. doi:10.1073/pnas.1011564107

Tytell, E. D., Carr, J. A., Danos, N., Wagenbach, C., Sullivan, C. M., Kiemel, T., Cowan, N. J. and Ankaralı, M. M. (2018). Body stiffness and damping depend sensitively on the timing of muscle activation in lampreys. *Integr. Comp. Biol.* **58**, 860-873. doi:10.1093/icb/icy042

Viana Di Prisco, G., Wallén, P. and Grillner, S. (1990). Synaptic effects of intraspinal stretch receptor neurons mediating movement-related feedback during locomotion. *Brain Res.* **530**, 161-166. doi:10.1016/0006-8993(90)90675-2

Videler, J. J. (1993). *Fish Swimming*. London: Chapman and Hall. ISBN 041240860.

Wardle, C. S., Videler, J. J. and Altringham, J. D. (1995). Tuning in to fish swimming waves: Body form, swimming mode and muscle function. *J. Exp. Biol.* **198**, 1629-1636. doi:10.1242/jeb.198.8.1629

Williams, T. L., Grillner, S., Smoljaninov, V. V., Wallén, P., Kashin, S. and Rossignol, S. (1989). Locomotion in lamprey and trout: the relative timing of activation and movement. *J. Exp. Biol.* **143**, 559-566. doi:10.1242/jeb.143.1.559